

Ion heat and momentum transport in the edge pedestal of ASDEX Upgrade

E. Viezzer¹, E. Fable¹, M. Cavedon^{1,2}, F. M. Laggner³, C. Angioni¹, M. G. Dunne¹, R. Dux¹, M. Bernert¹, A. Burckhart¹, R. M. McDermott¹, T. Odstrcil^{1,2}, T. Pütterich¹, F. Ryter¹, E. Wolfrum¹, the ASDEX Upgrade Team and the EUROfusion MST1 Team*

¹ Max Planck Institute for Plasma Physics, Garching, Germany

² Physik-Department E28, Technische Universität München, Garching, Germany

³ Institute of Applied Physics, TU Wien, Fusion@ÖAW, Vienna, Austria

Introduction

Edge localized modes (ELMs) are magnetohydrodynamic instabilities that occur at the plasma edge of high confinement (H-mode) plasmas. These bursty edge perturbations expel particles and energy from the pedestal region, leading to a transient degradation of the H-mode transport barrier. ELMs are thought to be driven by a complex interplay between the edge pressure gradient ∇p and current density j . The energy exhaust during an ELM (which lasts typically for 1–2 ms) can account for up to 30 % of the total stored energy in the plasma.

In this paper we present the temporal evolution of the ion and electron profiles during the ELM cycle. A comparison of the toroidal momentum and thermal energy losses is shown for a variety of H-mode plasmas with different conditions. Analysis of the ion heat transport at the plasma edge shows that the ion heat conductivity is close to the neoclassical level in high collisionality plasmas, while at lower collisionality the ion heat transport is observed to be a factor of ~ 2 higher in the pedestal region.

Profile evolution during an ELM cycle

The unique edge diagnostic suite available at ASDEX Upgrade (AUG) allows us to measure the edge kinetic profiles on a sub-ms to ms time-scale and with a spatial resolution of less than 5 mm, making it ideal to study the recovery of the profiles after an ELM crash. The temporal evolutions of the edge temperature, density and toroidal rotation profiles during the ELM cycle were analyzed in various H-mode discharges with low ELM frequency (<130 Hz). The parameter range for the analyzed dataset are toroidal magnetic field on-axis $B_t = 2.4\text{--}2.5$ T, plasma current $I_p = 0.8\text{--}1.0$ MA, triangularity $\delta = 0.2\text{--}0.34$, heating power 4.0–9.5 MW, fuelling level $\Gamma_D = 1.6\text{--}11.5 \times 10^{21} e^-/\text{s}$ and pedestal ion collisionalities (at $\rho_{pol} = 0.97$) $v_i^* = 0.2\text{--}2.5$.

In figure 1 example profiles of the electron temperature (T_e), density (n_e), ion temperature (T_i) and impurity toroidal rotation (v_{tor} , usually measured on boron at AUG) for two different pedestal ion collisionalities, $v_i^* = 0.32$ (black) and $v_i^* = 1.45$ (red), are shown. The low collisionality discharges were obtained with low D fuelling ($1.5\text{--}3.0 \times 10^{21} e^-/\text{s}$), high δ (~ 0.34) and

*See <http://www.euro-fusionscipub.org/eu-im>

medium heating power level (9 MW). Only data measured -4.5 ms up to -1.0 ms before the ELM crash are plotted. While the electron density is only slightly lower ($\sim 20\%$) at low v_i^* , the core electron and ion temperatures are roughly 50 % higher. Interestingly, v_{tor} changes sign at the plasma edge ($\rho_{pol} > 0.95$) and is in the counter-current direction at low collisionality (see figure 1(d)).

As shown, the H-mode ‘dip’ feature in the edge toroidal rotation profile [1] is maintained, but is shifted to negative values. The feature also appears to be wider, concurrent with a wider T_i pedestal (see figure 1(c)). Using the ELM synchronization technique, which sorts the measured data with respect to the onset of an ELM, the temporal behaviour of the profiles can be tracked during the entire ELM cycle. In figure 2 the values of n_e , T_e , T_i and v_{tor} at the radial position $\rho_{pol} = 0.97$ are plotted against the ELM onset time. Note that for n_e and T_e the measurements evaluated with the integrated data analysis approach [2] with a temporal resolution below 1 ms are used, while T_i and v_{tor} are measured with the standard edge CXRS system with a time resolution of 2.3 ms.

Previous ELM cycle studies revealed that the electron density and temperature exhibit different recovery timescales [3]. During the ELM both the n_e and T_e gradient are small, followed by five distinct phases in the T_e recovery, while the n_e recovery shows three phases [3]. After the initial ∇T_e recovery, the density recovers rapidly and typically reaches its pre-ELM value 4–5 ms after the ELM crash. The full T_e recovery usually evolves on a longer timescale. Figure 2 shows a similar behaviour of n_e and T_e as observed in [3] in both discharges. While T_e and T_i evolve on similar timescales in both discharges, n_e shows an initial fast recovery phase (3–4 ms after the ELM onset). The T_i crash seems to evolve on a slower timescale compared to T_e , however, note that the drop could be obscured by the temporal resolution of the edge CXRS system. At low v_i^* , n_e exhibits a second slow recovery phase to reach its pre-ELM value [4]. In this

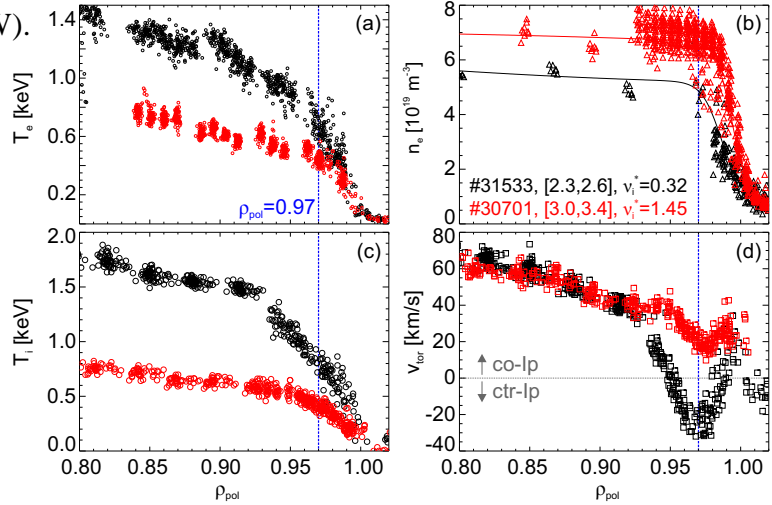


Figure 1: Plasma profiles at low (black) and high (red) v_i^* : (a) T_e , (b) n_e , (c) T_i , (d) v_{tor} .

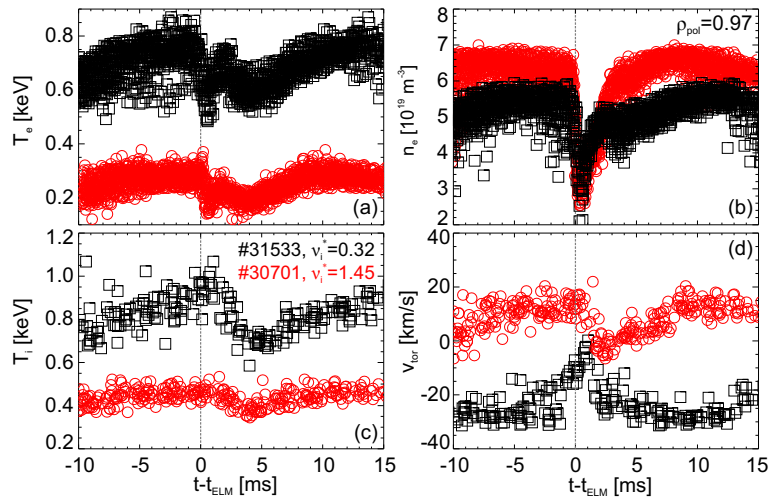


Figure 2: Temporal evolution of (a) T_e , (b) n_e , (c) T_i and (d) v_{tor} at $\rho_{pol}=0.97$ during the ELM cycle. $t-t_{ELM}=0$ denotes the ELM onset.

case, also the recovery of the edge impurity toroidal rotation to its pre-ELM value appears to be faster than the ion temperature recovery. At both collisionalities, the ELM crash induces a breaking of the edge plasma. Nonlinear modelling is required to study the dominant mechanism that is responsible for a faster restoration of the edge toroidal momentum compared to the heat transport. At higher v_i^* , the recovery times of n_e , T_e , T_i and v_{tor} to reach their pre-ELM values are similar and are on the order of ~ 6 ms [3, 5]. Note that at low v_i^* the average ELM energy loss per ELM is larger (by a factor of ~ 2 – 3) compared to high v_i^* plasmas.

Evaluating the relative losses in n_e , T_e , T_i and v_{tor} shows that the toroidal rotation exhibits a larger relative drop after the ELM compared to the drop in temperature and density profiles. The toroidal momentum and thermal energy losses are calculated by volume integrating the pre- and post-ELM profiles, i.e. only data where the full exposure time of the frame lies in the time windows $[-4.5, -1.0]$ ms and $[+0.5, +3.5]$ ms are used, respectively. Note that here the volume integral extends from $\rho_{pol} = 0.9$ to 1.0, i.e. the region which is mostly affected by the ELM. In all analyzed discharges, at both low and high v_i^* , the ejected relative thermal energy loss is smaller than the relative toroidal momentum loss (see figure 3), in agreement with previous analysis at JET with the carbon wall [6]. A possible explanation for the different behaviour in the ELM induced energy and momentum losses was given by the presence of neutrals in the pedestal and SOL region [7]. Dedicated experiments will be performed in the upcoming AUG campaign to test this hypothesis in an all-metal device.

Ion heat transport analysis

Extensive studies of the heat transport in the plasma core have been carried out in the past years, however, little focus was directed to the pedestal region due to lack of high-resolution diagnostics. Previous analysis of the temperature gradients measured at AUG were compared to simulations using the 2D fluid code B2.5 and showed that the pedestal ion heat transport coefficient in-between ELMs are consistent with neoclassical theory [8, 9].

In this work, the ion heat transport is studied using power balance analysis with ASTRA [10]. For the analysis dedicated discharges at low collisionality, where the ion and electron heat channels are not too strongly coupled, were selected. For the power balance analysis, the effects due to an ELM are excluded and only data from -5 ms up to -1 ms before the ELM onset are used. The analysis yields an edge ion heat conductivity on the order of $\chi_i^{PB} \sim 0.7$ m²/s (see figure 4(a)) and exhibits similar values as the electron heat conductivity (χ_e^{PB}). Note that the temporal evolution of T_i is taken into account for the evaluation of the heat flux and the χ^{PB} profiles shown in

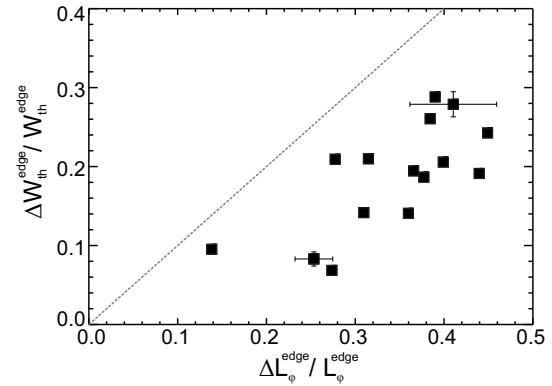


Figure 3: Relative loss in thermal energy plotted versus the relative loss in edge toroidal momentum.

figure 4 correspond to the temporal average in the analyzed time window. Comparison to the neoclassical profile calculated with NEO [11] (red) shows that at low v_i^* the ion heat transport is approximately a factor of ~ 2 higher than the neoclassical level at the plasma edge. Note that χ_i could be influenced by a possible residual effect of the ELM crash since at low v_i^* the T_i profile is still increasing until the next ELM occurs (see figure 2(c)).

At higher v_i^* (see figure 4(b)), the ion heat transport approaches the neoclassical level in the pedestal region, while further inwards it exceeds the neoclassical value by a factor of 4–5. Note that here the uncertainties are larger due to a stronger coupling between ion and electron heat channels. To quantify the differences between low and high v_i^* plasmas, this analysis will be extended to the upgraded edge CXRS diagnostic [13] which enables measurements with a time resolution down to $30\ \mu\text{s}$, thus allowing for detailed studies of the ion heat transport just after the onset of an ELM.

Conclusions

Analysis of the ELM synchronized profiles shows that the ejected relative toroidal momentum loss due to an ELM is larger than the relative loss in thermal energy. At low v_i^* the edge toroidal rotation recovers faster than the ion temperature after an ELM crash, indicating that first the momentum transport level is restored, followed by the heat transport level. Power balance analysis show that the ion heat transport in the pedestal region is near the neoclassical level at high v_i^* , while at low v_i^* , χ_i is a factor of 2 higher compared to the neoclassical value. A possible residual effect of the ELM may have an impact on χ_i at low v_i^* . Comparison to other neoclassical codes such as NEOART [12] are the subject of future work.

Acknowledgments This work has been carried out within the framework of the EUROfusion Consortium and has received funding from the Euratom research and training programme 2014–2018 under grant agreement No 633053. The views and opinions expressed herein do not necessarily reflect those of the European Commission. The support from the EUROfusion Researcher Fellowship programme under grant number WP14-FRF-IPP/Viezzer is gratefully acknowledged.

References

- [1] T. Pütterich *et al.*, PRL 102 025001 (2009)
- [2] R. Fischer *et al.*, FST 58 675 (2010)
- [3] A. Burkhart *et al.*, PPCF 52 105010 (2010)
- [4] F. M. Laggner *et al.*, P1.147 this conference
- [5] E. Viezzer *et al.*, PPCF 53 053005 (2013)
- [6] T. W. Versloot *et al.*, PPCF 52 045014 (2010)
- [7] T. W. Versloot *et al.*, PPCF 53 065017 (2011)
- [8] A. V. Chankin *et al.*, PPCF 48 839 (2006)
- [9] E. Wolfrum *et al.*, EPS conference (2007)
- [10] G. V. Pereverzev *et al.*, IPP Report (2002)
- [11] E. A. Belli *et al.*, PPCF 54 015015 (2012)
- [12] A. G. Peeters *et al.*, PoP 7 268 (2000)
- [13] M. Cavedon *et al.*, P1.130 this conference

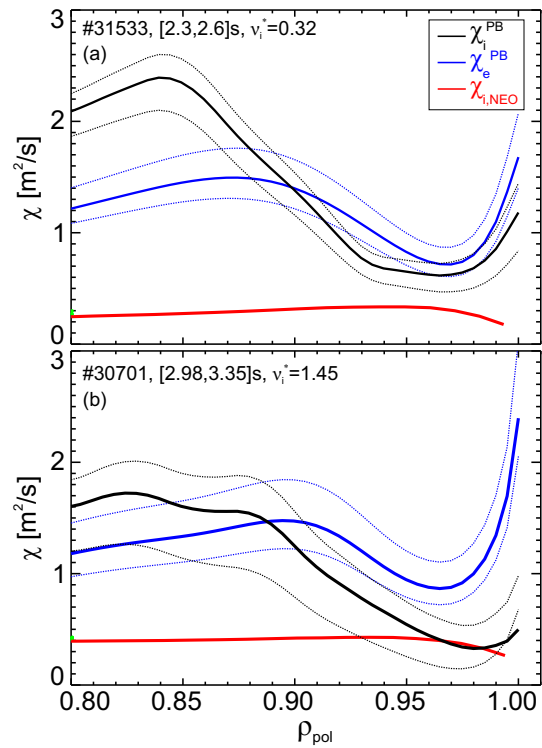


Figure 4: Ion (black) and electron (blue) heat conductivities determined via power balance. The neoclassical prediction is shown in red.